A GNSS/IMU/WSS/VSLAM Hybridization Using an Extended Kalman Filter

Amani Ben Afia, Anne-Christine Escher, Christophe Macabiau, Sébastien Roche

A GNSS/IMU/WSS/VSLAM Hybridization Using an Extended Kalman Filter

Amani BEN AFIA, Anne-Christine ESCHER, Christophe MACABIAU, Sébastien ROCHE
ENAC Telecom Lab, France

BIOGRAPHIES

Amani BEN AFIA graduated in 2012 as an Electronics engineer from ENAC (French National Civil Aviation School), Toulouse, France. Since 2013, she has been a PhD student in the Signal Processing and Navigation Research Group (SIGNAV) of ENAC. Her research focuses on developing multi-sensor fusion algorithms for the navigation in constrained environments.

Dr. Anne-Christine ESCHER graduated as an electronics engineer in 1999 from the ENAC in Toulouse, France. Since 2002, she has been working as a researcher and as a lecturer in the signal processing and navigation research group (SIGNAV) of the TELECOM Lab in the ENAC. She received her Ph.D. in 2003.

Dr. Christophe MACABIAU graduated as an electronics engineer in 1992 from the ENAC in Toulouse, France. Since 1994, he has been working on the application of satellite navigation techniques to civil aviation. He received his PhD in 1997 and has been in charge of the signal processing lab of ENAC since 2000.

Sébastien ROCHE graduated as an aeronautical engineer from the ISAE-ENSICA in 2010. He received his Ph.D. on reception algorithms in challenging environments in 2013 from the University of Toulouse. He has been working since 2015 in the navigation department of Airbus Defence and Space as a GNSS studies engineer.

ABSTRACT

Accurate positioning is nowadays a pre-requisite in many fields of applications. In Civil Aviation, accurate positioning is required for aircraft in precision approach or for vehicles moving on airport surfaces in order to guarantee their safety. Most of current positioning systems rely on the Global Navigation and Satellite System (GNSS). However, in constrained or semi-constrained environment such as airports, stand-alone GNSS navigation is quite vulnerable since the provided GNSS solution may be degraded by multipath resulting from the diffraction of GNSS signals on the airport obstacles, or even unavailable. A possible solution is to fuse information from different sensors in order to enhance the system performance. Since the targeted application is cost-sensitive, low-cost sensors will be used in this study. Therefore, the challenge of this paper is to achieve a high level of positioning accuracy using a low-cost solution.
In order to achieve our objective, a hybridization system fusing information from a GNSS receiver, an Inertial Navigation System (INS), a monocular camera and a Wheel Speed Sensor (WSS) is presented, and a loosely-coupled architecture based on an error-state Extended Kalman Filter (EKF) is proposed. Visual information is processed using the keyframe-based Visual Simultaneous Localization And Mapping (VSLAM) technique. The proposed architecture is centered on the INS and uses measurements from the other sensors. These aiding measurements are output by each navigation system after being processed independently. This paper focuses on the visual module and highlights its contribution to the enhancement of the navigation system performance.

I. INTRODUCTION

Vehicles moving on airport surfaces require a stringent positioning accuracy in order to guarantee their safety. The surveillance requirements in terms of accuracy, integrity, continuity and availability on airport surfaces are detailed in [1]. The position accuracy during manoeuvers on airport surfaces should not exceed few meters. In our work, this accuracy is targeted for airport ground vehicles. Stand-alone GNSS cannot always provide this required level of accuracy because of the possible signal degradation mainly due to multipath resulting from its diffraction on airport surfaces, or due to its blockage [2].

As an alternative to stand-alone GNSS, it has been shown that fusing information from different sensors results in an improved position robustness and accuracy if they have complementary advantages. In fact, by exploiting the complementarity of sensors, hybridization algorithms can improve the navigation solution with respect to that provided by each stand-alone sensor. The most widely implemented hybridization algorithms for land vehicles fuse GNSS measurements with inertial and/or odometric data [3] [4]. This way, these dead-reckoning (DR) sensors ensure the system continuity when GNSS information is unavailable and improve the system performance when GNSS signals are corrupted by multipath; and in return the GNSS limits the drift of DR solution if it is available. However the performance achieved by this hybridization

depends thoroughly on the quality of the DR sensor used especially when GNSS signals are degraded. Since the targeted application is cost-sensitive, low-cost sensors will be used in this study. Therefore, the challenge of this paper is to achieve a high level of accuracy with a low-cost solution, and some other complementary low-cost sensors should be employed to achieve the performance required.

In the last decades, cameras have become one of the most attractive positioning sensors. In fact it has been proven that vision techniques are capable of providing accurate navigation solution [5] while having reasonable cost. In general, vision systems reach very accurate results when using stereovision. However, the main drawback of such a configuration compared to a single camera is that in large-scale environments, the images captured by the cameras might contain objects placed too far. Processing these images does not allow recovering the depth values unless the stereo camera baseline is of few metres [6]. In addition to this compactness issue, a calibration issue arises when a multi-camera system is used and the calibration of a single camera is much easier [7]. Therefore, a single camera will be considered in this study. In case of a monocular vision module, a classical issue due to the projective nature of a single camera arises: the depth information of a 3D world point projected onto the image plane cannot be recovered using a single camera since a single 2D image point is the projection of an infinite number of 3D world points. This depth ambiguity results in a scale factor affecting the position estimated by the visual module and decreases dramatically its accuracy. Therefore, the visual navigation solution accuracy depends thoroughly on the good estimation of the scale factor.

Most of prior work focused on eliminating this scale problem in order to improve the visual solution either by using other sensors such as inertial [8], GNSS[9], and odometric measurements [10], or by using previously-mapped markers [11]. However, little work has considered the monocular vision module as a black box providing aiding measurements (position in undefined scale and scale free attitude) in a multi-sensor fusion framework. The proposed work in this paper focuses on this idea and uses visual information as aiding measurements in an integrated multi-sensor system aiming at providing a cost-effective and a robust navigation solution. In the proposed architecture, the INS is selected as the reference sensor since it provides a complete and continuous navigation solution including position, velocity and attitude. The INS estimation errors are corrected by GNSS, vision and WSS measurements using an error-state EKF based on a closed loop configuration and a loosely-coupled architecture. The visual scale factor is estimated in the filter state vector and is used after in the update step of the Kalman filter in order to make homogeneous the inertial and visual position. This way, vision provides accurate information to the fusion algorithm and in return, the other sensors help the visual module to overcome the scale factor issue.

This paper is organized as follows. First, an overview of the use of camera as a navigation sensor is performed. Then, the integrated navigation system is detailed and the fusion strategy is proposed. The equations of the process and measurement models are presented and discussed. Finally, the performance analysis of the proposed algorithm is performed. In particular, the results of the implemented GNSS/IMU/WSS/VSLAM are compared to the ones of the classical GNSS/IMU/WSS, GNSS/IMU in order to highlight the contribution of each sensor and particularly the camera, especially when the quality of the GNSS solution is degraded or when GNSS solution is unavailable.

II. CAMERA AS A NAVIGATION SENSOR

There are different ways to use the camera as a navigation sensor. In fact, mounted on board a vehicle, cameras can simply provide geometric information, such as distance or angle to a target detected in the image sequence, or process the information supplied by the images in order to provide an estimation of the position and orientation of the camera, referred to as the *camera pose*. This pose is expressed in a frame called *vision frame* described in section (**III.A**).

We focus in this study on the latter case where the camera is used as a pose estimation sensor. In this case, the vehicle motion is estimated based on the changes that occur in the images captured when the camera moves. In fact, motion is estimated based on the comparison of some specific object locations in the images. This comparison can be performed either with respect to a database previously built which means that the environment is already known, or between the images captured by the camera using the dead-reckoning principle for unknown environments. Since the development of a database is too heavy and too complex, this study focuses on the case where the environment is unknown.

A review and a classification of visual pose estimation techniques are performed in a previous work [12]. Generally, these techniques are based on the detection and tracking of salient zones of the images called *Features*. These techniques are classified into two main categories: *Visual Odometry* (VO) and *Visual Simultaneous Localization And Mapping* (VSLAM). Both techniques incrementally estimate the pose in the vision frame by examining the changes that motion induces on images taken by the camera(s). The only difference is that VO aims at estimating only the camera pose according to the displacement measured from the comparison of the image sequence. This comparison is performed by establishing matches between the features observed in the sequence of images. On the other hand, VSLAM not only provides an

estimation of the camera pose, but also builds at the same time the map of the environment in which the camera is moving. That is, after detecting features in an image, VSLAM determines the 3D feature positions and uses these reconstructed features in order to estimate the camera pose.

In this study, a keyframe-based VSLAM is used. This technique reconstructs features detected in some selected images called *Keyframes* and computes the camera pose using these features. Then a refinement process aiming at minimizing the re-projection errors of the reconstructed features is performed in order to improve jointly the estimation of the map and the camera pose. This process is called *Bundle Adjustment* [13]. More details on the use of camera as a navigation sensor are in [12]. Thanks to this refinement step, VSLAM has better performance than VO. Nonetheless its navigation solution not only drifts because of the DR principle, but also suffers from an unknown scale factor affecting the position when a monocular camera is used. These problems are handled in the proposed multi-sensor fusion architecture and the corrected visual information is, in turn, exploited to improve the system accuracy.

III. NAVIGATION FILTER

A. Muti-sensor System Design

The aim of this study is to develop a low-cost multi-sensor fusion system capable of providing accurate navigation information for ground airport vehicles.
The proposed architecture consists of a single frequency GNSS receiver, a low-cost Inertial Measurement Unit (IMU), a vision module processing the images of a single camera with the keyframe-based VSLAM technique and a WSS. The IMU is selected as the reference sensor since it is the only sensor continuously providing a complete navigation solution (position, velocity and attitude). As shown in **Figure 1**, the INS mechanization errors are corrected by the measurements of the other sensors. An error-state EKF is used in order to estimate the corrections that should be applied to the inertial navigation solution. The estimated IMU measurement errors are fed back to the mechanization since we have to deal with a low-cost IMU. Otherwise, as highlighted in [3], the mechanization can experience unbounded error growth, and the assumption of small errors used in the linearization process of the filter can be violated.

As mentioned previously, the proposed architecture uses GNSS, VSLAM and WSS as aiding sensors. It also exploits constraints reflecting the behaviour of the vehicle during navigation. These constraints consist mainly in considering that the vehicle moves only in the forward direction [14]. GNSS, if available, provides the vehicle position and velocity. The choice of processed GNSS data (position and velocity) instead of raw GNSS measurements (pseudo-ranges and pseudo-range rates) is justified by the fact that the airport can be assimilated to a semi-constrained environment. In such environments, we often meet the condition of having at least 4 satellites in view. In addition, loose coupling of GNSS with INS is much simpler, more robust and has faster processing time compared to tight coupling [15]. VSLAM provides the vehicle attitude in the vision frame, as well as its position given with an undefined scale k_v.

In order to be able to exploit the VSLAM attitude information, the orientation of the vision frame with respect to the local frame should be estimated. The VSLAM position information is used if the scale is also estimated. These two quantities are added to the state vector in order to be estimated.

Finally the WSS provides the forward vehicle velocity.

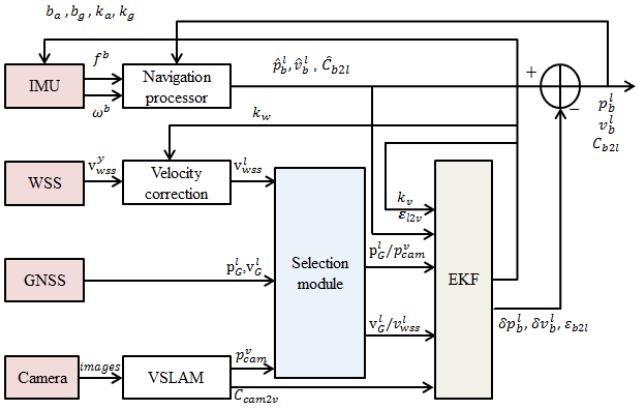

Figure 1: Multi-sensor system design

Due to the integration of such heterogeneous sensors, a special attention should be paid to the different coordinate systems associated to the sensors and the relationship between them. **Table 1** specifies, for each sensor, the outputs and the associated coordinate system.

As highlighted in [3] and [14] , it is preferred to express the position error in meters than in radians in order to avoid numeric instability inside the filter. Hence, the Local Tangent Plane is used as the reference system instead of the Latitude, Longitude and Height frame. As shown in **Figure 2**, the origin of this frame defined locally is chosen to be the initial position of the vehicle and its axes point towards the geographic East, North and Up directions (ENU). The velocity and the orientation are also expressed in this frame. In this study, we represent the orientation of a frame (α) w.r.t. a frame (β) by a $(3x3)$ rotation matrix denoted $\boldsymbol{C}_{\alpha 2\beta}$.

The WSS output is defined along the body frame axes as shown in **Figure 2**. This frame is rigidly attached to the

vehicle. The y-axis points to the forward direction, the z-axis points upwards and the x-axis completes the right-handed orthogonal frame.

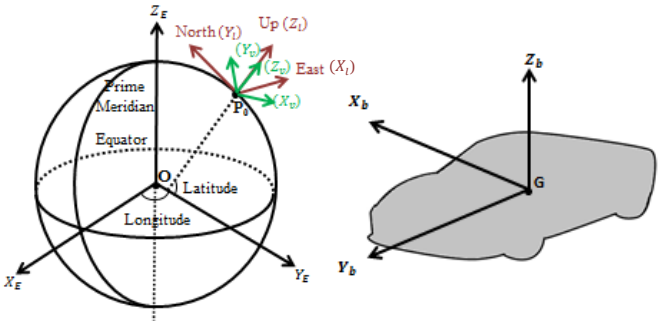

Figure 2: Reference frames

The VSLAM outputs are given with respect to the vision frame. The VSLAM is considered in this study as a black box providing the camera pose in the vision frame. Therefore, the vision frame orientation with respect to the local frame is unknown. However, its origin is assumed to be the initial position of the vehicle [15].

Nav. module	Output		Frame	Frame Origin
INS	INS Position	$\widehat{\boldsymbol{p}}_b^l$	Local ENU (l)	Initial vehicle position
	INS Velocity	$\widehat{\boldsymbol{v}}_b^l$		
	INS Attitude	$\widehat{\boldsymbol{C}}_{b2l}$		
GNSS	Antenna Position	$\widetilde{\boldsymbol{p}}_G^l$	Local ENU (l)	Initial vehicle position
	Antenna Velocity	$\widetilde{\boldsymbol{v}}_G^l$		
VSLAM	Camera Position	$\widetilde{\boldsymbol{p}}_{cam}^v$	Vision (v)	Initial vehicle position
	Camera Attitude	$\widetilde{\boldsymbol{C}}_{cam2v}$		
WSS	Rear Wheels Velocity	$\tilde{v}_w^y$	Body (b)	Vehicle center of mass

Table 1: Sensor outputs

The difference between the sensors lies also in their running rates. Normally, the INS has the highest rate followed by the camera. The WSS and the GNSS have the lowest rates. Regardless of the frame rate values, the filter integrates each aiding measurement as it comes and updates the state vector. The GNSS measurements considered of bad quality are removed. This selection is based on the Dilution Of Precision (DOP) as well as the C/N_0 values of the satellites. If the aiding sensors do not provide any measurement or if a GNSS measurement is removed based on the previously mentioned criteria, then the IMU measurements are used for propagating the state. If a sensor (WSS or camera) provides a measurement at the same time as GNSS and if the GNSS measurements were not rejected, then the filter selects the GNSS measurements since they are the most reliable measurement in good GNSS conditions.

B. Navigation Filter

Notations and assumptions

In this study, the notations with the hat ^ are estimated quantities and those with the tilde ~ are measured quantities. The notations without hat or tilde are actual quantities.

We assume that all the lever arms and orientation between the aiding sensors and the IMU are perfectly known and are measured before the navigation starts. The following notations are used:

- Lever arm between GPS antenna and IMU: $\Delta\boldsymbol{p}_G^b$
- Lever arm between camera and IMU: $\Delta\boldsymbol{p}_{cam}^b$
- Lever arm between WSS and IMU: $\Delta\boldsymbol{p}_w^b$
- Orientation of the camera w.r.t. $(\boldsymbol{b})$: $\boldsymbol{C}_{cam2b}$

Inertial Sensor Model

An IMU is at least composed of accelerometers and gyroscopes. The accelerometers measure the specific force and the gyroscopes measure the angular rate. The measurements are provided in the body frame. In this work, 3 accelerometers and 3 gyroscopes are used. These measurements are inevitably affected by errors. For a low-cost IMU, these errors mainly consist of biases, scale factors and noise. In this study, the inertial measurements are modelled by the following equations:

$$\tilde{\boldsymbol{f}}^b = (\boldsymbol{I_3} + \boldsymbol{k}_a) \cdot \boldsymbol{f}^b + \boldsymbol{b}_a + \boldsymbol{\eta}_a \quad (1)$$

$$\tilde{\boldsymbol{\omega}}^b = (\boldsymbol{I_3} + \boldsymbol{k}_g) \cdot \boldsymbol{\omega}^b + \boldsymbol{b}_g + \boldsymbol{\eta}_g \quad (2)$$

where $\tilde{\boldsymbol{f}}^b$ and $\tilde{\boldsymbol{\omega}}^b$ are respectively the measured specific force and angular rate in the body frame. $\boldsymbol{k}_a$ and $\boldsymbol{k}_g$ are the scale factors associated to the accelerometers. $\boldsymbol{b}_a$ and $\boldsymbol{b}_g$ are the biases, and $\boldsymbol{\eta}_a$ and $\boldsymbol{\eta}_g$ are the noises.

Vision measurement model

The VSLAM outputs are given in the vision frame. In order to build the vison module measurement model, these outputs should be expressed as a function of the INS mechanization outputs. This can be done using the following equations. We remind that $(\boldsymbol{v})$ and $(\boldsymbol{l})$ have the same origin, that the position provided by VSLAM has an undefined scale and that the attitude is scale free.

Position:

$$\hat{\boldsymbol{k}}_v \cdot \tilde{\boldsymbol{p}}_{cam}^v = \widehat{\boldsymbol{C}}_{l2v} \cdot \left(\widehat{\boldsymbol{C}}_{b2l} \cdot \Delta\boldsymbol{p}_{cam}^b + \widehat{\boldsymbol{p}}_b^l\right) + \boldsymbol{\eta}_V \quad (3)$$

with $\boldsymbol{\eta}_V$ is modeled as zero-mean, white and Gaussian noise.

Attitude:

$$\widetilde{\boldsymbol{C}}_{cam2v} = \widehat{\boldsymbol{C}}_{l2v} \cdot \widehat{\boldsymbol{C}}_{b2l} \cdot \boldsymbol{C}_{cam2b} \quad (4)$$

GNSS measurement model

GNSS provides position and velocity in $(\boldsymbol{l})$ frame. The GNSS measurement model taking into account the lever-arm is [3]:

Position

$$\widetilde{\boldsymbol{p}}_G^l = \widehat{\boldsymbol{p}}_b^l + \widehat{\boldsymbol{C}}_{b2l} \cdot \Delta \boldsymbol{p}_{GNSS}^b + \boldsymbol{\eta}_{G,p} \quad (5)$$

Velocity

$$\widetilde{\boldsymbol{v}}_G^l = \widehat{\boldsymbol{v}}_b^l + \widehat{\boldsymbol{C}}_{b2l} \boldsymbol{\Omega}_{lb}^b \Delta \boldsymbol{p}_G^b + \boldsymbol{\eta}_{G,v} \quad (6)$$

with

- $\boldsymbol{\Omega}_{lb}^b = \left(\widetilde{\boldsymbol{\Omega}}^{\mathrm{b}} - \boldsymbol{\Omega}_{il}^b\right)$, $\boldsymbol{\Omega}^{\mathrm{b}}$ and $\boldsymbol{\Omega}_{il}^b$ are respectively the skew-symmetric matrix of the gyro measurement $\widetilde{\omega}^b$and of ω_{il}^b.
- $\boldsymbol{\omega}_{il}^b = \boldsymbol{C}_{b2l}^T\left(\boldsymbol{\omega}_{ie}^l + \boldsymbol{\omega}_{el}^l\right)$, with $\boldsymbol{\omega}_{ie}^l$ is the earth rate and $\boldsymbol{\omega}_{el}^l$ is the transport rate resolved in $(\boldsymbol{l})$ frame.
- $\boldsymbol{\eta}_{G,p}$ and $\boldsymbol{\eta}_{G,v}$ are additive zero-mean, white and Gaussian noises whose variances are provided by the GNSS navigation module.

WSS measurement model

WSS provides velocity along the forward axis of $(\boldsymbol{b})$ frame. The measurement model of the WSS is given in by:

$$\widetilde{\boldsymbol{v}}_w^l = \widehat{\boldsymbol{C}}_{b2l}\left(1 + \hat{k}_w\right)\widetilde{\boldsymbol{v}}_w^b + \widehat{\boldsymbol{C}}_{b2l}\boldsymbol{\Omega}_{lb}^b \Delta \boldsymbol{p}_w^b + \boldsymbol{\eta}_w \quad (7)$$

with $\widetilde{\boldsymbol{v}}_w^b = [0 \quad \tilde{v}_w^y \quad 0]^T$, k_w is the WSS scale factor and $\boldsymbol{\eta}_w$ is the WSS noise modeled as zero-mean, white and Gaussian. The lateral and vertical velocities are set to zero. This is due to the motion constraints of a ground vehicle, called *Non-Holonomic Constraints* [14].

Sate Vector

The INS estimates the navigation parameters *i.e.* the position, velocity and attitude of the vehicle, and the aiding sensors allow the filter to estimate the errors of INS parameters as well as the errors of the inertial raw measurements.

The errors of the navigation parameters are defined by:

$$\delta \boldsymbol{p}_b^l = \widehat{\boldsymbol{p}}_b^l - \boldsymbol{p}_b^l \quad (8)$$

$$\delta \boldsymbol{v}_b^l = \widehat{\boldsymbol{v}}_b^l - \boldsymbol{v}_b^l \quad (9)$$

$$\widehat{\boldsymbol{C}}_{b2l} = (\boldsymbol{I} - \boldsymbol{E}_{b2l})\, \boldsymbol{C}_{b2l} \quad (10)$$

where $\boldsymbol{E}_{b2l}$ is the skew-symmetric matrix of the attitude error $\boldsymbol{\varepsilon}_{b2l} = [\varepsilon_E \quad \varepsilon_N \quad \varepsilon_U]$

Using the previous notations, a 21-element error state vector associated to INS is consequently used:

$$\delta \boldsymbol{x}_{INS} = \left[\delta \boldsymbol{p}_b^l \quad \delta \boldsymbol{v}_b^l \quad \boldsymbol{\varepsilon}_{b2l} \quad \delta \boldsymbol{b}_a \quad \delta \boldsymbol{b}_g \quad \delta \boldsymbol{k}_a \quad \delta \boldsymbol{k}_g\right]^T \quad (11)$$

Since we use processed measurements from GNSS, no state is associated to GNSS.

Vision position and WSS velocity are affected by the scale factor ambiguities. Vision attitude is exploited only if the orientation of $(\boldsymbol{v})$ w.r.t $(\boldsymbol{l})$ is known**.** These parameters should be estimated. The associated state vectors are therefore given by:

$$\delta \boldsymbol{x}_{Vision} = [\delta k_v \quad \boldsymbol{\varepsilon}_{l2v}]^T \quad (12)$$

$$\delta x_{wss} = \delta k_w \quad (13)$$

The full EKF state is the concatenation of the state vectors associated to each sensor. It is given by:

$$\delta \boldsymbol{x} = [\delta \boldsymbol{x}_{INS}{}^T \quad \delta x_{Vision}{}^T \quad \delta x_{wss}]^T \quad (14)$$

State transition model

The behavior of the navigation parameter errors can be obtained by perturbing the following INS mechanization equation using **Eq. (1-2)** and **Eq. (8-10)** and keeping only the first order terms:

$$\begin{bmatrix} \dot{\boldsymbol{p}}_b^l \\ \dot{\boldsymbol{v}}_b^l \\ \dot{\boldsymbol{C}}_{b2l} \end{bmatrix} = \begin{bmatrix} \boldsymbol{v}_b^l \\ \boldsymbol{C}_{b2l}\boldsymbol{f}^b - \left(2\boldsymbol{\omega}_{ie}^l + \boldsymbol{\omega}_{el}^l\right) \times \boldsymbol{v}_b^l + \boldsymbol{g}^l \\ \boldsymbol{C}_{b2l}\left(\boldsymbol{\Omega}^b - \boldsymbol{\Omega}_{il}^b\right) \end{bmatrix} \quad (15)$$

where $\boldsymbol{g}^l$ is local gravity including the Gravitation term and the centripetal term related to Earth rotation.

We model the inertial measurement bias and scale factor errors as Gauss-Markov process [15]:

$$\delta \dot{e}_{su} = -\frac{1}{\tau_{e_{su}}} \cdot \delta e_{su} + \eta_{e_{su}} \quad (16)$$

where e is the error ($e = b$ or $e = k$), s is the sensor ($s = a$ or $s = g$) and u is the $(\boldsymbol{b})$ frame axis ($u = x$, $u = y$ or $u = z$). $\tau_{e_{su}}$is the correlation time of the error e of the sensor s along the u-axis and $\eta_{e_{su}}$ is a zero-mean Gaussian noise.

The vision and WSS scale factor errors, as well as the orientation error of the vision frame with respect to the local frame, are modeled as constant states:

$$\delta \dot{k}_v = \eta_{kv} \quad (17)$$

$$\dot{\boldsymbol{\varepsilon}_{l2v}} = \boldsymbol{\eta}_{\epsilon} \quad (18)$$

$$\delta \dot{k_w} = \eta_{kw} \quad (19)$$

The models defined previously can be summarized to the following linearized continuous time sate transition model:

$$\dot{\delta \boldsymbol{x}} = \boldsymbol{F} \cdot \delta \boldsymbol{x} + \boldsymbol{G} \cdot \boldsymbol{u} \quad (20)$$

The expressions of F and G are given in the Appendix.

$$\boldsymbol{u} = [\boldsymbol{\eta}_a \quad \boldsymbol{\eta}_g \quad \boldsymbol{\eta}_{ba} \quad \boldsymbol{\eta}_{bg} \quad \boldsymbol{\eta}_{ka} \quad \boldsymbol{\eta}_{kg} \quad \eta_{kv} \quad \boldsymbol{\eta}_{\epsilon} \quad \eta_{kw}]^T \quad (21)$$

The corresponding process noise covariance matrix is given by:

$$\boldsymbol{Q} = \mathrm{cov}(\boldsymbol{u}) \quad (22)$$

The discrete time sate transition model assuming that F and G are constant over the time step between two consecutive state propagations Δt is given by:

$$\delta \boldsymbol{x}_{k+1} = \boldsymbol{\Phi}_k \cdot \delta \boldsymbol{x}_{k+1} + \boldsymbol{w}_k \quad (23)$$

with [3]

$$\boldsymbol{\Phi}_k = \boldsymbol{I} + \boldsymbol{F}.\Delta t \quad (24)$$

and

$$\mathbf{Q}_k = \mathrm{cov}(\boldsymbol{w}_k) = \boldsymbol{\Phi}_k \boldsymbol{G}\boldsymbol{Q}\boldsymbol{G}^{\boldsymbol{T}} \boldsymbol{\Phi}_k^T \, \Delta t \quad (25)$$

With the discrete state transition model, we can propagate the state using the prediction equations of the EKF. Since we are in a closed-loop configuration where the errors estimated by the EKF are fed back after the measurement update, the state vector should be reset to zero. Nonetheless, the state covariance is predicted using the equation:

$$\boldsymbol{P}_{k+1}^{-} = \boldsymbol{\Phi}_k \boldsymbol{P}_k \boldsymbol{\Phi}_k^T + \mathbf{Q}_k \quad (26)$$

Measurement models:

GNSS measurement model:

The position and velocity measurement vectors consist respectively in the difference between the GNSS position and the INS position denoted $\delta \boldsymbol{z}_{G,p}$, and the GNSS velocity and the INS velocity denoted $\delta \boldsymbol{z}_{G,v}$. In the case where the GNSS antenna and the IMU are placed in the same place, these measurement vectors are normally given by:

$$\delta \boldsymbol{z}_{G,p} = \boldsymbol{p}_G^l - \boldsymbol{p}_b^l \quad (27)$$

$$\delta \boldsymbol{z}_{G,v} = \boldsymbol{v}_G^l - \boldsymbol{v}_b^l \quad (28)$$

However, the lever-arm between the GNSS antenna and the IMU, denoted $\Delta \boldsymbol{p}_G^b$, should be accounted for. Using **Eq.(5-6)**, the measurement vector is given by:

$$\delta \boldsymbol{z}_{G,p} = \widetilde{\boldsymbol{p}}_G^l - \widehat{\boldsymbol{C}}_{b2l} \Delta \boldsymbol{p}_G^b - \widehat{\boldsymbol{p}}_b^l \quad (29)$$

$$\delta \boldsymbol{z}_{G,v} = \widetilde{\boldsymbol{v}}_G^l - \widehat{\boldsymbol{C}}_{b2l} \boldsymbol{\Omega}_{lb}^b \Delta \boldsymbol{p}_G^b - \widehat{\boldsymbol{v}}_b^l \quad (30)$$

Since we use an error-state EKF, the relationship between the measurement vector and the state can be written as:

$$\delta \boldsymbol{z}_{G,p} = \boldsymbol{H}_{G,p} \cdot \delta \boldsymbol{x} + \boldsymbol{\eta}_{G,p} \quad (31)$$

$$\delta \boldsymbol{z}_{G,v} = \boldsymbol{H}_{G,v} \cdot \delta \boldsymbol{x} + \boldsymbol{\eta}_{G,v} \quad (32)$$

with

$$\boldsymbol{H}_{G,p} = \left[-\boldsymbol{I}_3 \quad \mathbf{0}_3 \quad -\left(\widehat{\boldsymbol{C}}_{b2l} \Delta \boldsymbol{p}_G^b\right) \times \quad \mathbf{0}_{3x17}\right] \quad (33)$$

$$\boldsymbol{H}_{G,v} = \left[\mathbf{0}_3 \quad -\boldsymbol{I}_3 \quad -\left(\widehat{\boldsymbol{C}}_{b2l} \boldsymbol{\Omega}_{lb}^b \Delta \boldsymbol{p}_G^b\right) \times \quad \mathbf{0}_3 \quad \widehat{\boldsymbol{C}}_{b2l} \left(\Delta \boldsymbol{p}_G^b\right) \times \quad \mathbf{0}_{3x11}\right] \quad (34)$$

where the notation $(\boldsymbol{a}) \times$ means the skew-symmetric matrix of the $(3x3)$ vector $\boldsymbol{a}$.

WSS measurement model:

As for GNSS, the WSS velocity measurement is defined from **Eq.7**, taking into account the WSS scale factor [17]:

$$\delta \boldsymbol{z}_{w,v} = \widehat{\boldsymbol{C}}_{b2l} \left(1 + \hat{k}_w\right) \widetilde{\boldsymbol{v}}_w^b - \widehat{\boldsymbol{C}}_{b2l} \Omega_{lb}^b \Delta \boldsymbol{p}_w^b - \hat{v}_b^l \quad (35)$$

$$\boldsymbol{H}_{w,v} = [\mathbf{0}_3 | \quad -\boldsymbol{I}_3 | \quad \left(\widehat{\boldsymbol{v}}_b^l\right) \times | \quad \mathbf{0}_3 | \quad \widehat{\boldsymbol{C}}_{b2l} \left(\Delta \boldsymbol{p}_w^b\right) \times | \quad \mathbf{0}_{3x10} | \quad \left(\widehat{\boldsymbol{v}}_b^l + \widehat{\boldsymbol{C}}_{b2l} \boldsymbol{\Omega}_{lb}^b \Delta \boldsymbol{p}_w^b\right)] \quad (36)$$

Visual measurement model:

The visual module provides position and attitude measurements. These measurements are expression by **Eq.(3-4).** Therefore

$$\delta \boldsymbol{z}_{cam,p} = \hat{k}_v \, . \widetilde{\boldsymbol{p}}_{cam}^v - \widehat{\boldsymbol{C}}_{l2v} \cdot \left(\widehat{\boldsymbol{C}}_{b2l} \cdot \Delta \boldsymbol{p}_{cam}^b + \widehat{\boldsymbol{p}}_b^l\right) \quad (37)$$

$$\boldsymbol{H}_{cam,p} = [\widehat{\boldsymbol{C}}_{l2v} | \quad \mathbf{0}_3 | \quad \widehat{\boldsymbol{C}}_{l2v} \left(\widehat{\boldsymbol{C}}_{b2l} \Delta \boldsymbol{p}_{cam}^b\right) \times | \quad \mathbf{0}_{3x12} | \quad -\widetilde{\boldsymbol{p}}_{cam}^v | \quad \widehat{\boldsymbol{C}}_{l2v} \cdot \left(\widehat{\boldsymbol{C}}_{b2l} \cdot \Delta \boldsymbol{p}_{cam}^b + \widehat{\boldsymbol{p}}_b^l\right) | \quad 0] \quad (38)$$

$$\delta \boldsymbol{z}_{cam,att} = \begin{bmatrix} \tilde{\varphi}_{VSLAM} - \hat{\varphi}_{INS} \\ \tilde{\theta}_{VSLAM} - \hat{\theta}_{INS} \\ \tilde{\psi}_{VSLAM} - \hat{\psi}_{INS} \end{bmatrix} = \boldsymbol{H}_{cam,att} \delta \boldsymbol{x} + \boldsymbol{\eta}_{v,att} \quad (39)$$

where φ_{VSLAM}, θ_{VSLAM} and ψ_{VSLAM} describe the attitude of the vehicle using the VSLAM attitude output. In fact, using **Eq.4**, the vehicle attitude can be deduced from the camera attitude:

$$\left(\tilde{\boldsymbol{C}}_{b2l}\right)_{VSLAM} = \hat{\boldsymbol{C}}_{l2v}^{T} \cdot \tilde{\boldsymbol{C}}_{cam2v} \cdot \boldsymbol{C}_{cam2b}^{T} \quad (40)$$

Using the expression of C_{b2l} defined in the Appendix:

$$\tilde{\varphi}_{VSLAM} = -\arctan\left(\frac{\left(\tilde{\boldsymbol{C}}_{b2l}^{31}\right)_{VSLAM}}{\left(\tilde{\boldsymbol{C}}_{b2l}^{33}\right)_{VSLAM}}\right) \quad (41)$$

$$\tilde{\theta}_{VSLAM} = \arcsin\left(\left(\tilde{\boldsymbol{C}}_{b2l}^{32}\right)_{VSLAM}\right) \quad (42)$$

$$\tilde{\psi}_{VSLAM} = \arctan\left(\frac{\left(\tilde{\boldsymbol{C}}_{b2l}^{12}\right)_{VSLAM}}{\left(\tilde{C}_{b2l}^{22}\right)_{VSLAM}}\right) \quad (43)$$

The same angle definition is applied for $\hat{\varphi}_{INS}$, $\hat{\theta}_{INS}$ and $\hat{\psi}_{INS}$ deduced from the rotation matrix $\widehat{\boldsymbol{C}}_{b2l}$ outputted by the INS mechanization. By applying **Eq.10**, we find:

$$\hat{\theta}_{INS} = \arcsin\left(\varepsilon_N \hat{C}_{b2l}^{12} - \varepsilon_E \hat{C}_{b2l}^{22} + \hat{C}_{b2l}^{32}\right) \quad (44)$$

$$\hat{\psi}_{INS} = \arctan\left(\frac{\hat{C}_{b2l}^{12} + \varepsilon_U \hat{C}_{b2l}^{22} - \varepsilon_N \hat{C}_{b2l}^{32}}{-\varepsilon_U \hat{C}_{b2l}^{12} + \hat{C}_{b2l}^{22} + \varepsilon_E \hat{C}_{b2l}^{32}}\right) \quad (45)$$

where $\hat{C}_{b2l}^{ij}$ is the (i,j) component of matrix $\widehat{\boldsymbol{C}}_{b2l}$.
The measurement matrix $\boldsymbol{H}_{cam,att}$ is computed by differentiating the expressions of the three angles with respect to ε_E, ε_N and ε_U:

$$\boldsymbol{H}_{cam,att} = \begin{bmatrix} 0_{1x6} & H_{17} & H_{18} & 0 & 0_{1x17} \\ 0_{1x6} & H_{27} & H_{28} & 0 & 0_{1x17} \\ 0_{1x6} & H_{37} & H_{38} & 1 & 0_{1x17} \end{bmatrix} \quad (46)$$

with:

$$H_{17} = \frac{\hat{C}_{b2l}^{21}\hat{C}_{b2l}^{33} - \hat{C}_{b2l}^{23}\hat{C}_{b2l}^{31}}{\left[\hat{C}_{b2l}^{31}\right]^2 + \left[\hat{C}_{b2l}^{33}\right]^2} \quad (47)$$

$$H_{18} = \frac{\hat{C}_{b2l}^{13}\hat{C}_{b2l}^{31} - \hat{C}_{b2l}^{11}\hat{C}_{b2l}^{33}}{\left[\hat{C}_{b2l}^{31}\right]^2 + \left[\hat{C}_{b2l}^{33}\right]^2} \quad (48)$$

$$H_{27} = \frac{-\hat{C}_{b2l}^{22}}{\sqrt{1 - \left[\hat{C}_{b2l}^{32}\right]^2}} \quad (49)$$

$$H_{28} = \frac{\hat{C}_{b2l}^{12}}{\sqrt{1 - \left[\hat{C}_{b2l}^{32}\right]^2}} \quad (50)$$

$$H_{37} = \frac{-\hat{C}_{b2l}^{12}\hat{C}_{b2l}^{32}}{\left[\hat{C}_{b2l}^{12}\right]^2 + \left[\hat{C}_{b2l}^{22}\right]^2} \quad (51)$$

$$H_{38} = \frac{-\hat{C}_{b2l}^{22}\hat{C}_{b2l}^{32}}{\left[\hat{C}_{b2l}^{12}\right]^2 + \left[\hat{C}_{b2l}^{22}\right]^2} \quad (52)$$

Filter modes and update

The previous section defines the measurement models for each aiding sensor. Since the processing rate of each sensor is different from the other and since the different rates are not necessarily multiples of each other, then we can identify 7 running modes:

- INS only mode (for state covariance propagation since we are in closed-loop)
- INS/VSLAM
- INS/WSS
- INS/GNSS
- INS/VSLAM/WSS
- INS/VSLAM/GNSS
- INS/WSS/GNSS
- INS/VSLAM/WSS/GNSS

For each mode, the full measurement vector/matrix is the concatenation of the available measurement vectors/matrices. The measurement covariance is the diagonal matrix whose elements are the variances of the available measurements.

Let $\delta z, H$ and R be respectively the full measurement vector, measurement matrix and measurement covariance matrix. Then, the update is performed using the Kalman filter equations:

$$K_{k+1} = P_{k+1}^{-} H_{k+1}^{T} \cdot \left[H_{k+1} P_{k+1}^{-} H_{k+1}^{T} + R_{k+1}\right]^{-1} \quad (53)$$

$$\delta \hat{x}_{k+1}^{+} = K_{k+1} \delta z_k \quad (54)$$

$$P_{k+1}^{+} = P_{k+1}^{-} - K_{k+1} \cdot H_{k+1} \cdot P_{k+1}^{-} \quad (55)$$

IV. EXPERIMENTS AND RESULTS

The algorithm is tested using GNSS and inertial data collected in an environment similar to airport. GNSS data is given by the GPS stand-alone mode of a Ublox-6 running at **1Hz**. Inertial measurements are obtained using an Xsens Mti IMU running at **100 Hz**. In a first step, VSLAM and WSS are simulated from the reference data using **Eq.(3-4)** and **Eq.7** with respective rates of **50Hz** for the VSLAM and **10Hz** for the WSS. In a second step, a 1280x1024 forward looking camera was mounted on the roof of the car. The video is processed using the VSLAM algorithm. The reference trajectory is determined using the NovAtel SPAN equipment [17]. **Figure 3** shows the equipment used for the measurement campaign. For simplicity reasons and since we target a vehicular application, only the horizontal performance will be analyzed.

Figure 3: measurement campaign equipment

A. Simulated VSLAM data

The vision scale factor is modeled as drifting linearly over time as shown in **Figure 4**. This model is not necessarily good since the visual scale factor has only spatial drift [18]. In fact, the vision scale only changes if new or different features are observed, and it keeps constant if the same features are observed. But since we are in outdoor environment, the observed features are always different and the time drift model can therefore be appropriate. We assume that the noise on the visual position is zero-mean, white and Gaussian with a standard deviation of **2m**. The noise on the attitude angles provided by the SLAM is assumed to have a standard deviation of **1°**.

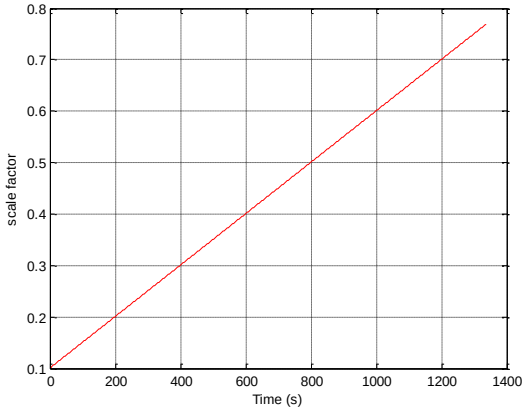

Figure 4: Vision scale factor drift

Figure 5 illustrates a comparison between the reference, the GPS and the VSLAM trajectories in the horizontal plane. We remind that VSLAM outputs are given in the $(\boldsymbol{v})$ frame defined up to a rotation and a scale factor with respect to the $(\boldsymbol{l})$ frame.

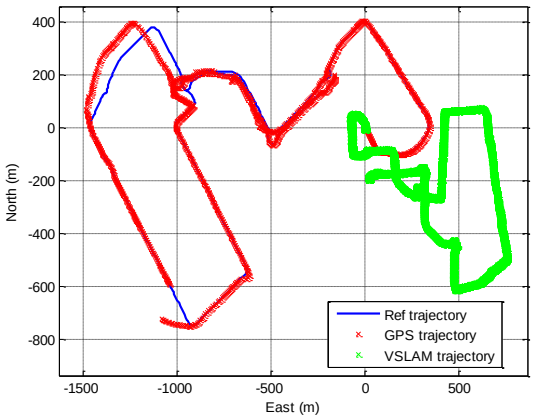

Figure 5: Horizontal trajectories

A comparison between the navigation performances of each of the following fusion algorithms is done in this section in order to highlight the contribution of each sensor to the improvement of the navigation performance:

- GPS
- GPS/IMU
- GPS/IMU/WSS
- GPS/IMU/WSS/VSLAM

Only the horizontal parameters will be analyzed since they are the most important parameters for land vehicle navigation.

Figure 6 and **Figure 7** illustrate a comparison of the horizontal position errors in the West-East and South-North directions given by the different systems.

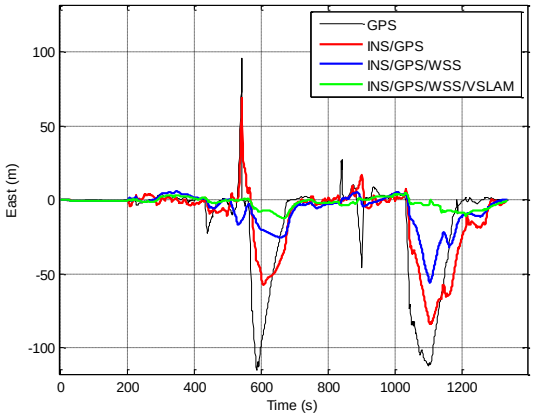

Figure 6: Horizontal West-East error

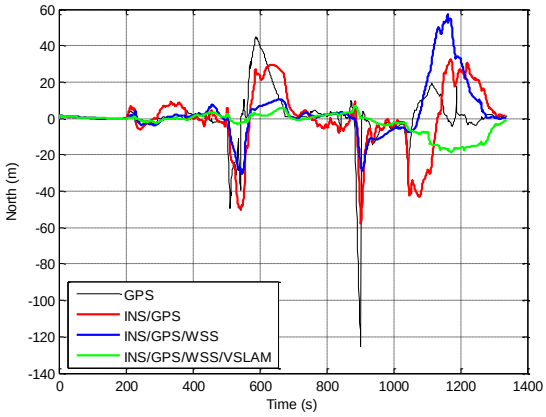

Figure 7: Horizontal South-North error

Each time a sensor is added, the navigation performance is improved. The errors in both West-East and South-North directions decrease dramatically when the sensors are added. A comparison of the West-East error statistics is performed in **Table 2**.

Algorithm	Mean (m)	STD (m)	Max (m)
GPS	13.01	31.56	115.3
GPS/INS	-11.09	22.33	83.59
GPS/INS/WSS	-6.34	11.65	55.88
GPS/INS/WSS/VSLAM	-1.84	3.61	12.17

Table 2: West-East error statistics

Finally a comparison between the headings outputted by each fusion algorithm is illustrated in **Figure 8**. It is clear that the heading aiding of the VSLAM improves dramatically the heading estimation. However, a simulation of zero-mean Gaussian error on the attitude outputted by the SLAM is a very optimistic assumption. Real data should be used in order to validate the model.

On the other hand, the use of WSS improves the estimation of the heading. This improvement is due to the correlation that exists between the attitude and the velocity. This correlation is expressed into the F matrix of the Kalman filter process model.

In the case of INS/GPS/WSS/VSLAM, the vision scale factor is estimated and is reinserted to the filter in order to be used in the update step. **Figure 9** shows the estimation of this scale factor by the developed EKF. If the estimation of this parameter is wrong, then the VSLAM position measurement will be wrong and will introduce a high error in the filter. That is why, the covariance matrix of the VSLAM position measurement depends thoroughly on the variance of the scale factor outputted by the EKF. In order to take into account this dependency, the measurement covariance matrix is multiplied by the scale variance. This improves the performance of the filter.

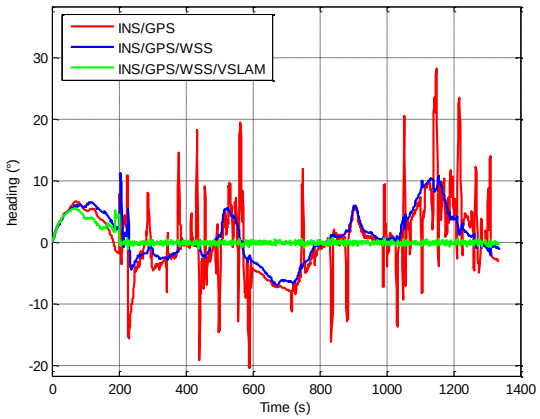

Figure 8: Heading error

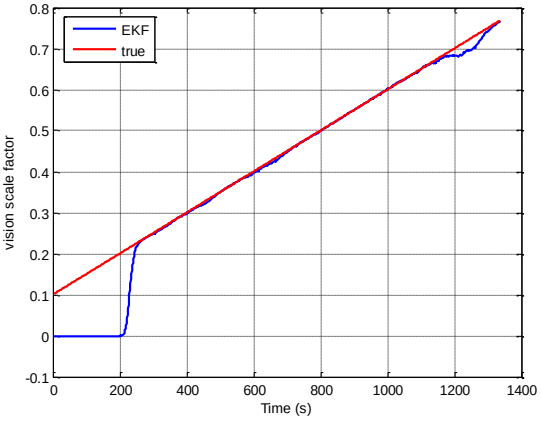

Figure 9: Vision scale factor estimation

In the first 205s, the vehicle is at rest. Since the VSLAM algorithm starts when the vehicles starts moving, then the use of the algorithm, and therefore the estimation of the scale factor starts after the vehicle moves. The convergence of the scale is achieved in 55s.

B. Real VSLAM data

The video taken by the camera is processed using the VSLAM algorithm. The comparison of the trajectory given by the VSLAM with the reference trajectory is performed in **Figure 10**. It shows clearly that the SLAM trajectory is affected by a scale factor. A zoom on the VSLAM trajectory in **Figure 11** shows that in addition to the scale problem, this trajectory is turned with respect to the reference trajectory.

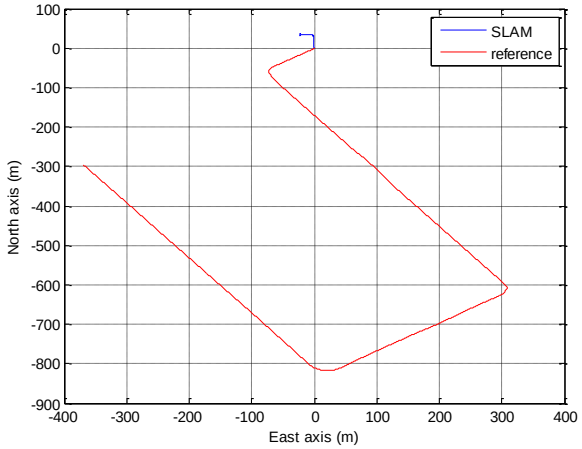

Figure 10: Reference and VSLAM trajectories

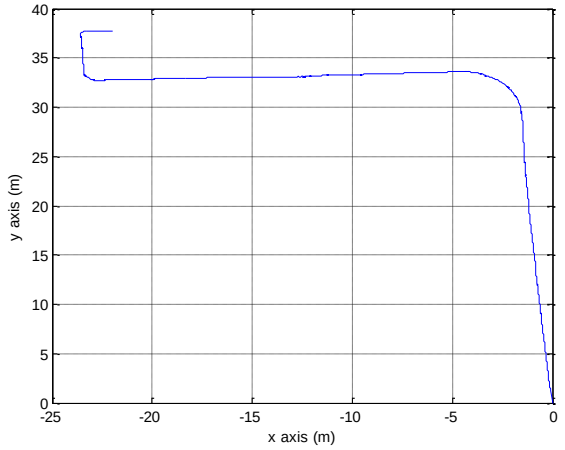

Figure 11: Zoom on VSLAM trajectory in (*v*)

As for simulated data, a comparison between the accuracy of the different navigation algorithms is illustrated in **Figure 12** and **Figure 13**. It shows that, even if the VSLAM trajectory is affected by a scale factor and a rotation, the use of this information improves the performance of the navigation system. This is highlighted in **Figures 14** and **Figure 15** where the scale factor and the rotation angle (2D case) are well estimated by the Kalman filter. The improvement of the navigation performance using the VSLAM is shown by **Table 3** in which a comparison of the West-East error statistics is performed.

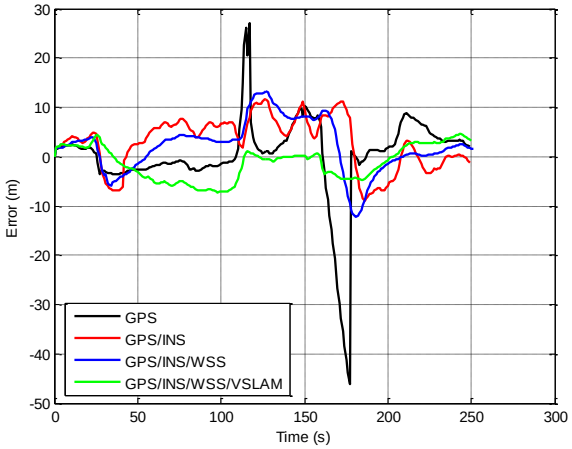

Figure 12: Horizontal West-East error

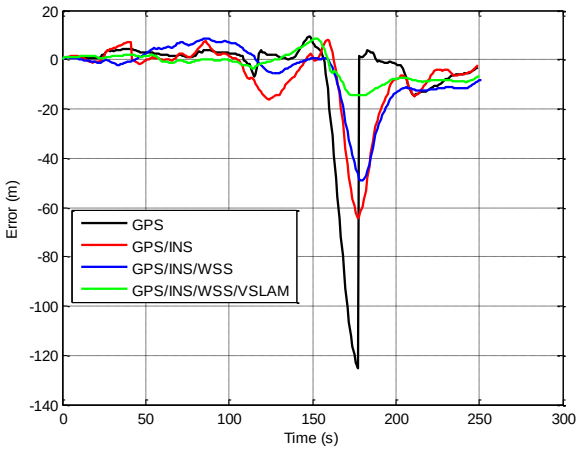

Figure 13: Horizontal South-North error

Algorithm	Mean (m)	STD (m)	Max (m)
GPS	0.18	8.72	46.03
GPS/INS	2.87	5.2	11.72
GPS/INS/WSS	2.19	5.2	13.16
GPS/INS/WSS/VSLAM	-1.12	3.47	7.2

Table 3: West-East error statistics

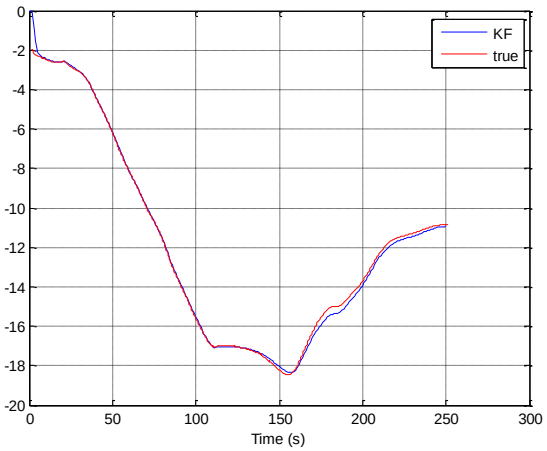

Figure 14: Vision scale factor estimation

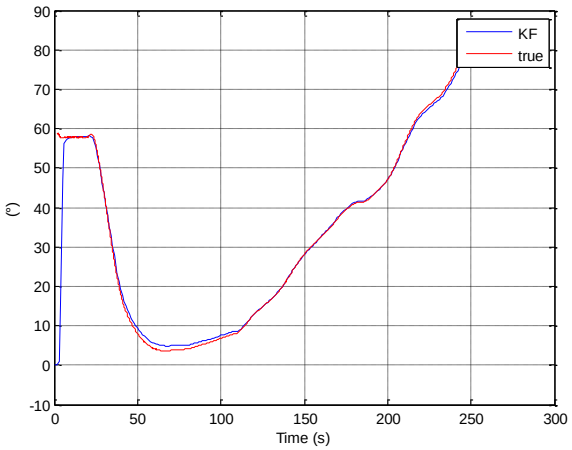

Figure 15: Local-vision frame rotation angle

Finally, a GNSS outage is simulated on the entire trajectory in order to test the performance of our algorithm with only dead-reckoning sensors. **Figure 16** and **Figure 17** show that after 250s, the drift is about **20m** with the use of visual information. **Table 4** gives the West-East error statistics in the case of GNSS removal and shows that it is possible to get a good accuracy with low-cost sensors.

Algorithm	Mean (m)	STD (m)	Max (m)
INS	3520	3051	8943
INS/WSS	351	241.8	669.7
INS/WSS/VSLAM	9.6	9.7	20.7

Table 4: West-East error statistics

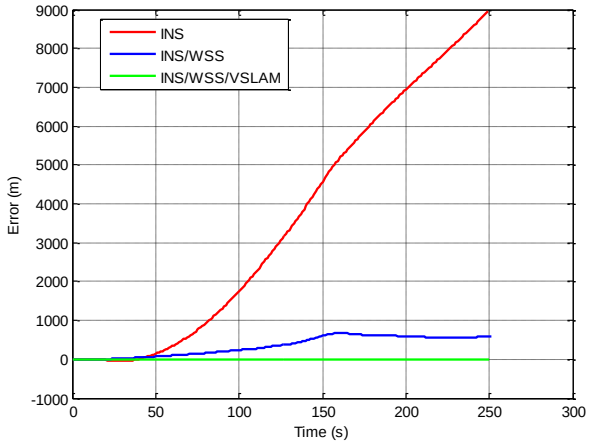

Figure 16: Horizontal West-East error

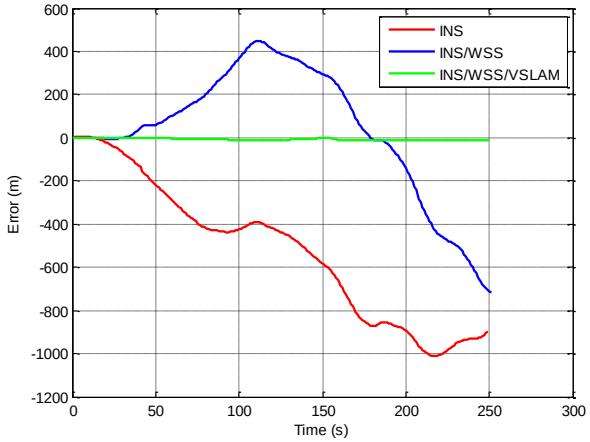

Figure 17: Horizontal South-North error

CONCLUSION

The current paper introduces a navigation system fusing low-cost sensors in order to improve the navigation parameter estimation for vehicles moving on airport surfaces. Results show that the use of a GPS/INS system is not sufficient to reach a high level of accuracy. The integration of complementary sensors such as the VSLAM providing position and attitude and the WSS providing velocity improves dramatically the navigation system performances. This was shown using simulated and real data. The possibility of having more than a measurement makes the system able to select the measurements according to their quality which improves the estimation of the navigation solution. This is the primary results of a study focusing on sensor integration. The next step will be to improve the fusion algorithm by using, for example, the filter innovation and the redundancy of measurements in order to exclude measurements having a large error. This can be done especially when GNSS raw measurements are

used. This allows us to exclude the faulty GNSS measurements which may improve the filter performance.

AKNOWLEDGMENT

We would like to thank the French DGE for funding this project as well as M3Systems and the Architecture & IC Design, Embedded Software Department of CEA Saclay.

REFERENCES

[1] ICAO, *Manual on advanced surface movement guidance and control systems (A-SMGCS)* - DOC9830 AN/452, First Edition 2004

[2] Y.S. Park, S. Pullen, P. Enge: "*A Study of Severe Multipath Errors for the Proposed GBAS Airport Surface Movement Application*", Proceedings of the 23rd International Technical Meeting of The Satellite Division of the Institute of Navigation (ION GNSS 2010), Portland, OR, September 2010, pp. 2661-2671

[3] E.H. Shin: "*Accuracy improvement of low cost INS/GPS for land applications*", PhD Thesis, Department of Geomatics Engineering, University of Calgary, 2001.

[4] M. Spangenberg, V. Calmettes, D. Kubrak, and O. Julien, "*Optimized low-cost HSGPS/IMU/WSS land vehicle navigation system for urban navigation*," in Proceedings of the 20th International Technical Meeting of the Satellite Division of the Institute of Navigation (ION GNSS '07), pp. 70–78, U.S. Institute of Navigation, Fort Worth Tex, USA, September 2007.

[5] D. Nistér,O. Naroditsky, J. Bergen: "*Visual odometry for ground vehicle applications*", Journal of Field Robotics, 2006, 23, (1), pp.3-20

[6] S. Hong, J.B. Song, J.H. Baek, J.K. Ryu.: "*Visual odometry for outdoor environment using a downward-tilting camera and self-shadow removal algorithm*", Proc. IEEE Int. Conf. Control, Automation and Systems (ICCAS), 2012, pp.960-963

[7] H. Strasdat, J. M. M. Montiel, and A. Davison, "*Scale drift-aware large scale monocular SLAM*," in Proc. of Robotics: Science and Systems (RSS), 2010.

[8] G. Nutzi, S. Weiss, D. Scaramuzza and R. Siegwart: "*Fusion of IMU and vision for absolute scale estimation in monocular SLAM*", Journal of Intelligent and Robotic Systems, **61**(1–4), 287–299.

[9] D. Dusha, L. Mejias: "*Attitude observability of a loosely-coupled GPS/Visual Odometry Integrated Navigation Filter*", Proc. Australasian Conf. Robotics and Automation, 2010

[10] A. Eudes, S. Naudet-Collette, M. Lhuillier,M. Dhome: "*Weighted Local Bundle Adjustment and Application to Odometry and Visual SLAM Fusion*", Proc. British Machine Vision Conference, BMVA Press, 2010, pp.25.1-25.10

[11] F. Lamberti, A. Sanna, G. Paravati, P. Montuschi, V. Gatteschi, and C. Demartini: "*Mixed marker-based/marker-less visual odometry system for mobile robots*", International Journal of Advanced Robotic Systems, 10, 2013

[12] A. Ben-Afia, L.Deambrogio, D. Salos, et al: "*Review and classification of vision-based localisation techniques in unknown environment"* , IET Radar, Sonar & Navigation, Volume 8, Issue 9, December 2014, p. 1059 – 1072

[13] C. Engles, H. Stewénius, D. Nistér: "*Bundle adjustment rules*", Proc. Symp. Photogrammetric Computer Vision, 2006

[14] S. Sukkarieh: " *Low Cost, High Integrity, Aided Inertial Navigation Systems for Autonomous Land Vehicles*" Ph.D. Thesis, Australian Centre for Field Robotics, Dept. of Mechanical and Mechatronic Engineering, The University of Sydney, 2000

[15] A. Angrisano: "*GNSS/INS Integration Methods*", PhD thesis, University of Naples Parthenope, 2010

[16] A. Eudes: "*Localisation et cartographie simultanées par ajustement de faisceaux local : propagation d'erreurs et réduction de la dérive à l'aide d'un odomètre*", PhD thesis, University of Blaise Pascal - Clermont-Ferrand II , 2011.

[17] *l* Seo, J, Lee, H.K., Lee, J.G and Park, C.G., (2006), "*Lever Arm Compensation for GPS/INS/Odometer Integrated System*", Inter. Journal of Contr., Automat. and Systems, vol. 4, no. 2, pp. 247-254..

[18] *http://www.novatel.com/assets/Documents/Manuals/om-20000139.pdf.*

[19] S. Weiss: S. Weiss: "*Vision based navigation for micro helicopters*", PhD thesis, ETH Zurich, 2012.

Appendix
State transition Model in the ENU frame

Definitions and Notations

In order to build the state transition model, some parameters should first be defined:

- The vehicle latitude, longitude and height are respectively denoted φ, λ and h
- The vehicle velocity in the (l) frame is represented by the vector $\boldsymbol{v}_b^l = [v_E \quad v_N \quad v_U]^T$
- The vehicle attitude is defined by the roll, pitch and heading respectively denoted ϕ , θ and ψ.
- The meridian and transverse radii of curvature in the earth ellipsoid respectively denoted R_m and R_n.
- The relationship between ϕ , θ and ψ, and C_{b2l} is given by :

$$\boldsymbol{C}_{b2l} = \begin{bmatrix} c\phi c\psi + \mathrm{s}\,\phi\,\mathrm{s}\,\theta\,\mathrm{s}\,\psi & \mathrm{c}\,\theta\,\mathrm{s}\,\psi & \mathrm{s}\,\phi\,\mathrm{c}\,\psi - \mathrm{c}\,\phi\,\mathrm{s}\,\theta\,\mathrm{s}\,\psi \\ -\mathrm{c}\,\phi\,\mathrm{s}\,\psi + \mathrm{s}\,\phi\,\mathrm{s}\,\theta\,\mathrm{c}\,\psi & \mathrm{c}\,\theta\,\mathrm{c}\,\psi & -\mathrm{s}\,\phi\,\mathrm{s}\,\psi - \mathrm{c}\,\phi\,\mathrm{s}\,\theta\,\mathrm{c}\,\psi \\ -\mathrm{s}\,\phi\,\mathrm{c}\,\theta & \mathrm{s}\,\theta & \mathrm{c}\,\phi\,\mathrm{c}\,\theta \end{bmatrix}$$

with c and s are respectively cosine and sine.

State transition model:

The state transition equation is given by:

$$\dot{\delta \boldsymbol{x}} = \boldsymbol{F} \cdot \delta \boldsymbol{x} + \boldsymbol{G} \cdot \boldsymbol{u}$$

The computation of the state transition matrix for INS states gives

$$\boldsymbol{F}_{INS} = \begin{bmatrix} F_{pp} & F_{pv} & 0_3 & 0_3 & 0_3 & 0_3 & 0_3 \\ F_{vp} & F_{vv} & F_{ve} & C_{b2l} & 0_3 & C_{b2l} \cdot F^b & 0_3 \\ F_{ep} & F_{ev} & -\Omega_{il}^l & 0_3 & -C_{b2l} & 0_3 & -C_{b2l} \cdot W^b \\ 0_3 & 0_3 & 0_3 & \beta_{ba} & 0_3 & 0_3 & 0_3 \\ 0_3 & 0_3 & 0_3 & 0_3 & \beta_{bg} & 0_3 & 0_3 \\ 0_3 & 0_3 & 0_3 & 0_3 & 0_3 & \beta_{sa} & 0_3 \\ 0_3 & 0_3 & 0_3 & 0_3 & 0_3 & 0_3 & \beta_{sg} \end{bmatrix}$$

With

$$\boldsymbol{F}_{pp} = \begin{bmatrix} \frac{V_U}{R_n + h} - \frac{V_N tan(\varphi)}{R_m + h} & \frac{V_E tan(\varphi)}{R_m + h} & \frac{-V_E}{R_n + h} \\ 0 & \frac{V_U}{R_m + h} & \frac{-V_N}{R_m + h} \\ 0 & 0 & 0 \end{bmatrix}$$

$$\boldsymbol{F}_{pv} = \boldsymbol{I_3}$$

$$\boldsymbol{F}_{vp} = \begin{bmatrix} 0 & F_{vp}^{12} & F_{vp}^{13} \\ 0 & F_{vp}^{22} & F_{vp}^{23} \\ 0 & F_{vp}^{32} & F_{vp}^{33} \end{bmatrix}, \text{ with}$$

$$F_{vp}^{12} = \frac{2\omega_e(v_N cos(\varphi) + v_U\, sin(\varphi))}{R_m + h} + \frac{v_E v_N}{(R_n + h)(R_m + h)\, cos^2(\varphi)}$$

$$F_{vp}^{13} = \frac{v_E v_U}{(R_n + h)^2} - \frac{v_E v_N\, tan(\varphi)}{(R_n + h)^2}$$

$$F_{vp}^{22} = \frac{-2\omega_e v_E\, cos(\varphi)}{R_m + h} - \frac{v_E^2}{(R_n + h)(R_m + h)\, cos^2(\varphi)}$$

$$F_{vp}^{23} = \frac{v_N v_U}{(R_m + h)^2} + \frac{v_E^2 \tan(\varphi)}{(R_n + h)^2}$$

$$F_{vp}^{32} = -\frac{2\omega_e\, v_E sin(\varphi)}{R_m + h}$$

$$F_{vp}^{33} = \frac{-v_E^2}{(R_n + h)^2} - \frac{v_N^2}{(R_m + h)^2} + \frac{2g^l}{R + h}$$

$$F_{vv} = \begin{bmatrix} F_{vv}^{11} & F_{vv}^{12} & F_{vv}^{13} \\ F_{vv}^{21} & F_{vv}^{22} & F_{vv}^{23} \\ F_{vv}^{31} & F_{vv}^{32} & 0 \end{bmatrix}, \text{ with}$$

$$F_{vv}^{11} = \frac{v_N\, tan(\varphi) - v_U}{R_n + h}$$

$$F_{vv}^{12} = \frac{v_E\, tan(\varphi)}{R_n + h} + 2\omega_e\, sin(\varphi)$$

$$F_{vv}^{13} = -2\omega_e\, cos(\varphi) - \frac{v_E}{R_n + h}$$

$$F_{vv}^{21} = \frac{-2v_E\, tan(\varphi)}{R_n + h} - 2\omega_e\, sin(\varphi)$$

$$F_{vv}^{22} = \frac{-v_U}{R_m + h}$$

$$F_{vv}^{23} = \frac{-v_N}{R_m + h}$$

$$F_{vv}^{31} = \frac{2v_E}{R_n + h} + 2\omega_e\, cos(\varphi)$$

$$F_{vv}^{32} = \frac{2v_N}{R_m + h}$$

$$F_{ve} = \left(C_{b2l} f^b\right) \times$$

$$\boldsymbol{F}_{ep} = \begin{bmatrix} 0 & 0 & \frac{v_N}{(R_m + h)^2} \\ 0 & -\frac{\omega_e \sin(\varphi)}{R_m + h} & \frac{-v_E}{(R_n + h)^2} \\ 0 & \frac{\omega_e \cos(\varphi)}{R_m + h} + \frac{v_E}{(R_n + h)(R_m + h)\cos^2(\varphi)} & \frac{-v_E \tan(\varphi)}{(R_n + h)^2} \end{bmatrix}$$

$$\boldsymbol{F}_{ev} = \begin{bmatrix} 0 & \dfrac{-1}{R_m + h} & 0 \\ \dfrac{1}{R_n + h} & 0 & 0 \\ \dfrac{\tan(\varphi)}{R_n + h} & 0 & 0 \end{bmatrix}$$

The full state transition matrix is given by:

$$F = \begin{bmatrix} F_{INS} & 0_{21x5} \\ 0_{5x21} & 0_{5x5} \end{bmatrix}$$

And the G matrix is given by:

$$G = \begin{bmatrix} 0_{3x3} & 0_{3x3} & 0_{3x17} \\ C_{b2l} & 0_{3x3} & 0_{3x17} \\ 0_{3x3} & -C_{b2l} & 0_{3x17} \\ 0_{17x3} & 0_{17x3} & I_{17x17} \end{bmatrix}$$